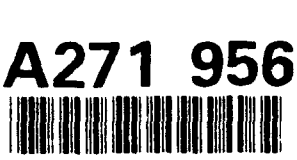

ARMY RESEARCH LABORATORY

Biaxial Flexural Testing of a Carbon Fiber Reinforced Epoxy Composite

Nikos Tsangarakis and Barmac K. Taleghani

ARL-TR-221

October 1993

The findings in this report are not to be construed as an official Department of the Army position unless so designated by other authorized documents.

Citation of manufacturer's or trade names does not constitute an official endorsement or approval of the use thereof.

Destroy this report when it is no longer needed. Do not return it to the originator.

REPORT DOCUMENTATION PAGE

Form Approved
OMB No. 0704-0188

1. AGENCY USE ONLY (Leave blank)	2. REPORT DATE	3. REPORT TYPE AND DATES COVERED
	October 1993	Final Report

4. TITLE AND SUBTITLE
Biaxial Flexural Testing of a Carbon Fiber Reinforced Epoxy Composite

5. FUNDING NUMBERS

6. AUTHOR(S)
Nikos Tsangarakis and Barmac K. Taleghani

7. PERFORMING ORGANIZATION NAME(S) AND ADDRESS(ES)
U.S. Army Research Laboratory
Watertown, MA 02172-0001
ATTN: AMSRL-MA-DB

8. PERFORMING ORGANIZATION REPORT NUMBER
ARL-TR-221

9. SPONSORING/MONITORING AGENCY NAME(S) AND ADDRESS(ES)
U.S. Army Research Laboratory
2800 Powder Mill Road
Adelphi, MD 20783-1197

10. SPONSORING/MONITORING AGENCY REPORT NUMBER

11. SUPPLEMENTARY NOTES

12a. DISTRIBUTION/AVAILABILITY STATEMENT
Approved for public release; distribution unlimited.

12b. DISTRIBUTION CODE

13. ABSTRACT (Maximum 200 words)

The response of a 3501-6 resin composite to biaxial flexural loading was assessed using disk specimens. The composite was cross-ply reinforced with continuous carbon fibers with a volume content of 60%. Under monotonic flexural loading, the formation of delaminations limited the useful range of the composite's deformation to a biaxial tensile strain of 0.0067. Under cyclic flexural loading and for a fatigue life of 10^6 cycles, the useful strain range was limited to 0.003. The latter strain is only 19% of the composite's uniaxial tensile strain to failure. Fatigue failure mechanisms included delaminations, matrix cracking, fiber, and possible fiber bundle debonds. Some delaminations were identified with ultrasonic C-scanning.

14. SUBJECT TERMS	15. NUMBER OF PAGES
Biaxial loading, Composites, Fatigue, Flexure of composites	18
	16. PRICE CODE

17. SECURITY CLASSIFICATION OF REPORT	18. SECURITY CLASSIFICATION OF THIS PAGE	19. SECURITY CLASSIFICATION OF ABSTRACT	20. LIMITATION OF ABSTRACT
Unclassified	Unclassified	Unclassified	UL

NSN 7540-01-280-5500

Standard Form 298 (Rev. 2-89)
Prescribed by ANSI Std. Z39-18
298-102

Contents

Figures

Tables

Introduction

The need to reduce weight in structural applications has led to the development of various new composite materials. Because of the lack of a well established database these new materials cannot yet be utilized to their full potential. A good database should include properties assessed under biaxial loading. In an earlier publication (1), a disk specimen was introduced to assess the response of a cross-ply, metal matrix composite to biaxial flexural loading. This test procedure and specimen geometry were originally used by other investigators for isotropic materials. The composite had a 6061 aluminum matrix of 70 GPa modulus and 290 MPa strength. The reinforcement was continuous silicon carbide fibers with a 386 GPa modulus and 3 GPa strength. The composite's fiber volume content was 45% to 47%. This composite's leading failure mechanism under monotonic loading or low cycle fatigue was fiber breakage. For high cycle fatigue, the main failure mechanism was matrix shear cracking.

The present work considers the response to biaxial tensile loading of a cross-ply composite of a low modulus (4.4 GPa), low strength (70 MPa) 3501-6 resin matrix which is reinforced with high modulus (248 GPa) and high strength (4 GPa) continuous carbon fibers. The composite's fiber volume content was 60%. The failure mechanisms were sought and an attempt was made to identify the generated damage nondestrutively. The performance of the organic composite is compared with that of the aluminum composite in order to understand how the biaxial response relates to basic material properties.

Material, Test Specimens, and Experimental Procedures

A composite plate with 16 layers of 3501-6 resin prepreg was prepared in-house. The prepreg contained 60% by volume HERCULES AS-4 continuous carbon fibers. The composite plate's lay up was $(O_2/90_2/O_2/90_2)_S$. The graphite/epoxy plate stock was 30 cm x 30 cm, and its thickness varied between 1.68 mm and 2.56 mm. The plate's thickness increased near its geometrical center. The plate had five randomly distributed dents of irregular shapes which reached a diameter of 2 mm and a depth of 0.2 mm.

The properties of the HERCULES AS-4 continuous carbon fiber and of the 3501-6 resin (as provided by the manufacturer) are listed in Tables 1 and 2, respectively. The composite properties shown in Table 3 were determined by E. T. Camponeshi, Jr. (2) and Daniel and Lee (3).

Table 1. Properties of Hercules AS-4 continuous carbon fiber

Ultimate Tensile Strength (UTS)	4 (GPa)
Elastic Modulus (E)	248 (GPa)
Strain to Fracture (e_f)	0.0165
Diameter	0.007 (mm)
Density	1.8 (gr/cm^3)

Table 2. Properties of the 3501-6 resin

Ultimate Tensile Strength (UTS)	70 (MPa)
Elastic Modulus (E)	4.4 (GPa)
Strain to Fracture (e_f)	0.017

Table 3. 3501-6 Resin/AS-04 carbon/60$_f$ composite laminate properties

Unidirectional Composite	
Elastic Modulus E_{11} (Parallel to the Fibers)	115 (GPa) (2)
Elastic Modulus E_{22} (Perpendicular to the Fibers)	11 (GPa) (2)
Major Poisson's Ratios	$v_{12} = v_{13} = 0.32$ (2)
Ultimate Longitudinal Tensile Strain	$e_{11} = 0.0156$ (3)
Ultimate In-plane Shear Strain	$e_{12} = 0.0057$ (3)
Cross-Ply $(0_2/90_2)_S$ Composite (3)	
Elastic Modulus - Parallel to 0^o Fibers (E_{11})	73.6 (GPa)
Ultimate Unixial Tensile Strength (UTS)	1.112 (GPa)
Ultimate Uniaxial Tensile Strain (e_f)	0.0155

NOTES: The first index of Poisson's ratios is parallel to the loading direction.
Numbers in brackets indicate the appropriate references.

Twenty disks were cut from the composite plate with a cylindrical hollow diamond drill using an appropriate fluid; e.g., TOOLMATE, as a coolant and lubricant and at a 3500 rpm cutting speed. These disks had a diameter of 50.8 mm and were used to conduct the biaxial flexural tests. The average disk thickness was 2.25 ± 0.2 mm. This average thickness was estimated from measurements on 19 disks. Each measurement was made at the center of the disk. The maximum thickness variability on a given disk was ± 0.14 mm.

Four straight specimens (2.5 cm x 25 cm) were also cut from the composite plate. These coupons were reinforced with aluminum end tabs (5 cm long) and were used to assess the elastic constant (E_{11}) and the strain and stress to failure under uniaxial tension. The length of these coupons was parallel to the 0^o fibers and the test procedure was the ASTM D 3039 *Tension Testing*.

Monotonic and cyclic biaxial flexural tests were conducted in a 90 KN load capacity, servohydraulic test machine. Four disks were tested under monotonic and 14 disks under cyclic biaxial flexural loading. To conduct a biaxial flexure test, the composite disk was positioned on a steel supporting ring that had outside and inside diameters of 50.8 mm and 48.8 mm, respectively. Load was transferred to the center of the disk with a 12.2 mm diameter and 25 mm long steel cylinder (see Figure 1). The displacement of the loading pin (W) was monitored with the machine's actuator displacement transducer. The displacement of the loading train without a specimen was only 0.025 mm at 1.8 KN load.

Strain measurements were conducted with 1 mm x 1 mm, 350 ohm resistance strain gages. These gages were positioned on the convex face of the disk (during loading), parallel to the 0^{o} fibers and at the disk's center. Thus, the strain gages were loaded in tension during testing. Strain measurements with Poisson's gages were conducted during biaxial loading to determine the relative magnitudes of the two principal tensile strains e_{xx} (parallel to the 0^{o} fibers) and e_{yy} (parallel to the 90^{o} fibers). Monotonic tests were conducted at a displacement rate of 1 mm/min. Fatigue tests were conducted at a frequency of 1 Hz and strain ratio of 0.1 (minimum over maximum cyclic strains). The initial 10 cycles were conducted under manual machine control. The load strain relationship was monitored with a digital oscilloscope and the load was raised appropriately so as to keep the strain range constant during cyclic loading.

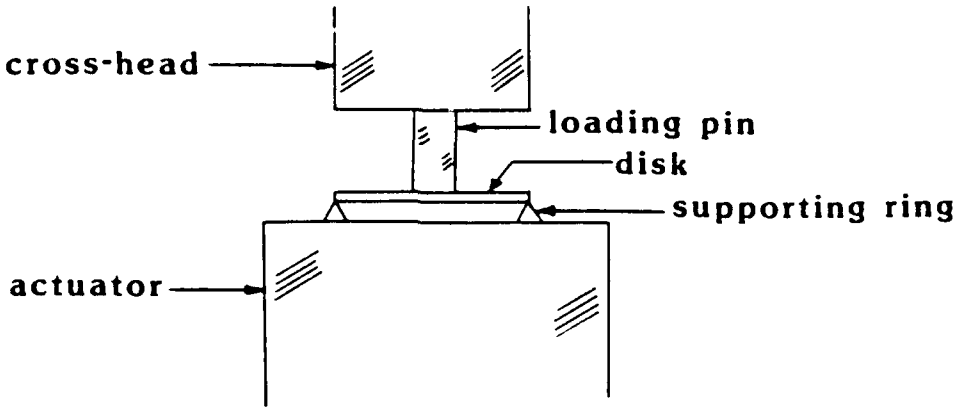

Figure 1. Loading arrangement for biaxial flexure

Nondestructive inspections (NDI) were conducted to identify the extent of the damage which was introduced in the composite disks due to the biaxial loading. The techniques employed were X-ray radiography, Eddy current mapping, and ultrasonic C-scanning. The nature of the damage was identified with traditional metallographic procedures.

Test Results

Monotonic Loading

The monotonic uniaxial tension testing of the straight coupons produced elastic modulus (E_{11}) values similar to that found by Daniel and Lee (3) and shown in Table 3. However, the ultimate tensile stresses and strains were much smaller than those shown in Table 3. The ultimate tensile strength was 418 ± 75 (MPa) and the ultimate tensile strain was 0.0067 ± 0.0012. The lower stress and strain values were probably the results of premature failures which, with the exception of one, occurred at the grips and not within the coupons' gage lengths.

A typical relationship between the applied load and the resulting biaxial tensile strain e_{xx} is depicted in Figure 2. Note that the curve is convex downward which is indicative of a stiffening process. The initial stiffness (tangent modulus) was 296 (KN/cm/cm), and the stiffness at a load of 2.2 KN was 434 (KN/cm/cm). The relationship was elastic up to 2.2 KN load and 0.0067 strain. At this strain, a *load instability* occurred

(see Figure 2) which was accompanied by an audible sound and an instantaneous decrease of the load by 450 N. The strain at instability was 43% of the composite's uniaxial tensile strain to failure (see Table 3). Although the original curve was resumed after the load instability with continuing loading, unloading from strains greater than 0.0067 resulted in a residual strain. The latter strain could be indicative of some composite damage which was generated during or after the load instability. The stiffening of the curve continued with loading beyond the point of load instability. The final failure of the composite disk occurred by partial (through the disk's thickness) piercing of the disk by the loading pin. The pin had split the disk into two parts. One part of the disk was fully penetrated by the pin while the other was not at all. Penetration had stopped at the beginning of the central double layer (90^{o} fibers). The fracture surfaces of the failed disk are shown in Figure 3. The peak load and the loading pin's displacement were 4.493 KN and 2.72 mm, respectively. During the monotonic biaxial loading of another disk, a load instability was noticed at a strain of 0.008. This latter strain is 52% of the composite's uniaxial tensile strain to failure. This disk was unloaded and cut with a diamond disk saw at several locations. The cross sections were polished through #600 grit paper and examined under low magnification (10X to 50X). Two cracks with planes parallel to the plies were found. Such cracks will be referred hereafter as *shear cracks*. One shear crack was located at the interface of the first 0^{o} double layer and the first 90^{o} double layer on the tension of the disk. The crack had an elliptic shape and was symmetric about the disk's center. Part of the crack is shown in Figure 4a. This crack was not detected by ultrasonic C-scanning or X-ray radiography. The second shear crack was located in the middle (through thickness) of the second double layer of the 0^{o} fibers (see Figure 4b). This crack was approximately 14 mm x 14 mm off the disk's center and was detected by C-scanning but not by the X-ray radiography. The third disk failed by shear cracking at a strain of 0.0074. Finally, the fourth disk did not exhibit a load instability but instead was penetrated fully by the loading pin at a peak load of 4.2 KN and 2.5 mm pin displacement.

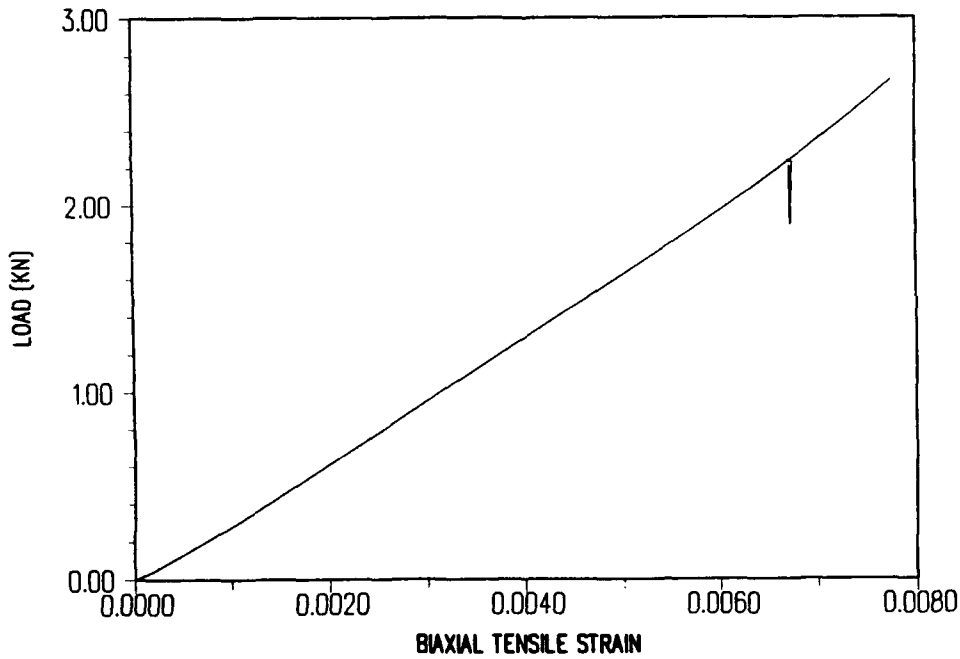

Figure 2. Load versus biaxial tensile strain

(a)

(b)

Figure 3. Fracture surfaces of pierced disk

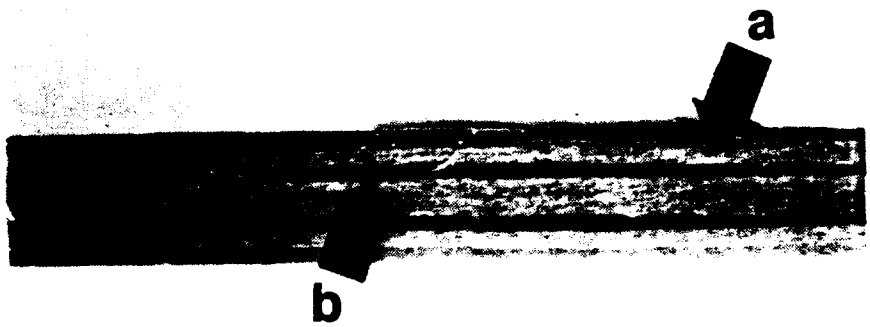

(a)

(b)

Figure 4. Shear cracks - delamination

Because the formation of *shear cracks* did not always occur within consistent boundaries, it was not possible to establish a unique failure pattern. Because of this uncertainty, failure under monotonic loading was said to have occurred whenever a minimal decrease of 10% of the instantaneous load was observed during testing. Since the minimal strain at which such a load instability was observed was 0.0067, it will be assumed that this strain represents the lower limit of the biaxial strain to failure of the composite under montonic tensile loading. This biaxial tensile strain limit is only 43% of the composite's uniaxial tensile strain to failure (0.0155 (3)).

The strain measurements with Poisson's gages indicated that during the biaxial tensile loading the two principal strains e_{xx} and e_{yy} were equal. This relationship was also found for a cross-ply aluminum composite by Tsangarakis and Pepi (1). The relationship holds true prior to introduction of damage in the composite disk.

Cyclic Biaxial Loading

The relationship between the cyclic biaxial tensile strain range and the composite's fatigue life is depicted in Figure 5. Open symbols represent failures while solid symbols indicate runouts. The dashed line represents the envelope below where no composite failure was observed. Fatigue failure was considered to have occurred whenever a minimal decrease of 10% of the maximal cyclic load was necessary in order to maintain a constant cyclic strain range. This failure definition is similar to that for monotonic loading and is independent of the nature of the failure mechanism. The strain endurance limit under biaxial cyclic tension for 10^6 cycles of fatigue life approached 0.003. This limit is only 19% of the composite's uniaxial strain to failure under monotonic loading which is 0.0155 (3) (see Table 3).

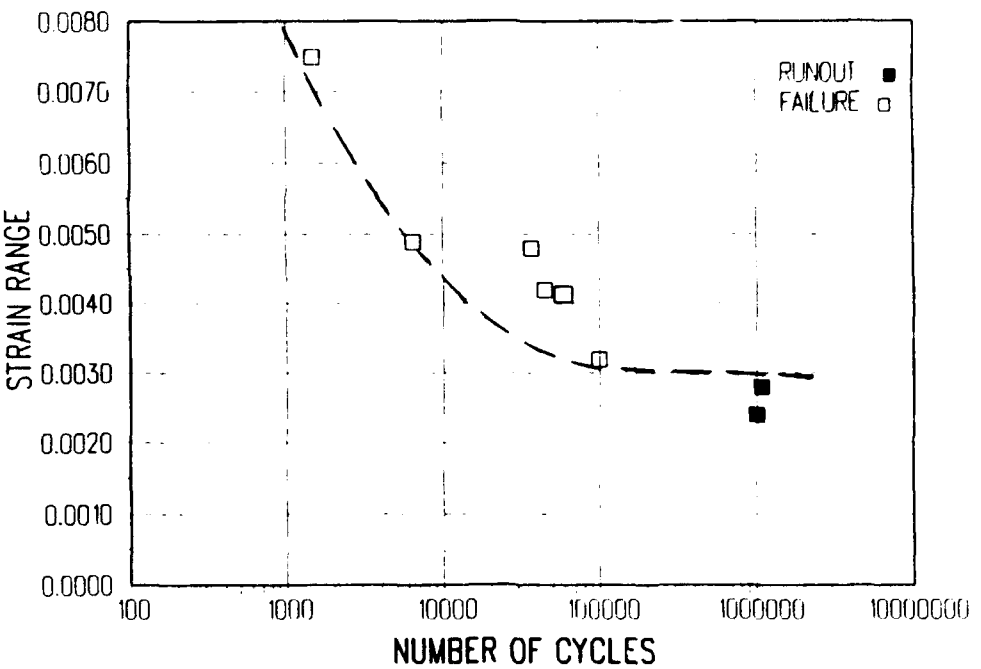

Figure 5. Fatigue life versus strain range

The relationship between the displacement of the loading pin and the resulting strain was linear, as shown in Figure 6. Each point shown in this figure represents a pair of the maximal cyclic displacement W and the corresponding maximal cyclic strain e_{xx} of an individual disk. The dashed line represents the least square fit of all data points. The little data scatter is probably due to the variation of the composite's thickness, which was discussed earlier (see the Material, Test Specimens, and Experimental Procedures Section). Thus, both the pin's displacement W and the strain e_{xx} may be

used as independent parameters to evaluate the response of the composite to the biaxial loading. However, since the strain e_{xx} represents a local response and the displacement W represents a global response, the linearity of the relationship is expected to be destroyed after the introduction of damage in the composite.

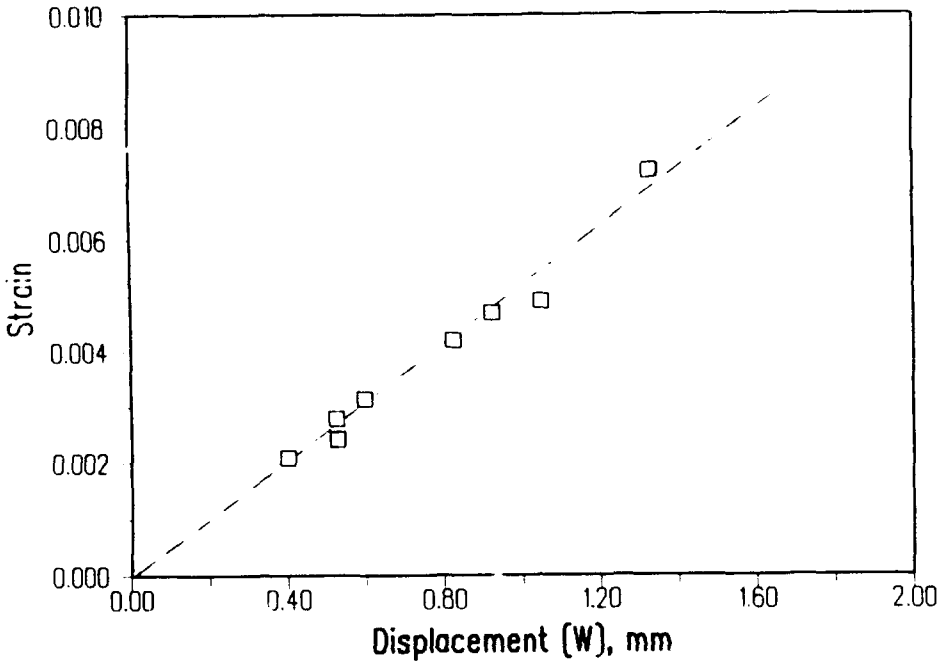

Figure 6 Strain - displacement relationship.

All the failed disks had at least one shear crack (see Figure 4). All shear cracks were found in the tension sides of the disks (during flexure). In addition to shear cracks, other defects were also found. Metallographic examination of a disk which had failed after 50,000 cycles at 0.0052 cyclic strain range revealed debonded fibers and numerous matrix cracks. These debonded fibers and cracks were in the outermost ply in the tension side of the disk and perpendicular to the ply (see Figure 7a). All defects of this type appeared within 6 mm from the disks' centers (see Figures 3 and 7b). Similar matrix cracks and debonded filaments appeared in another disk after 1100 cycles at a cyclic strain range of 0.0072. A different defect type is depicted in Figure 8. Defects of this latter type (see Figure 4a, arrow b) represented areas where a bundle of fibers and the associated matrix had separated (debonded) from the surrounding composite. These debonded areas were up to 5 mm long and were found throughout the volume of the fatigued disks. Examination of untested disks indicated that these debonded areas could have been formed during the cutting of the composite and not necessarily be the result of fatigue. It is noted, however, that if these debonded areas existed in the composite disks during their biaxial cyclic loading, they could act as areas of stress concentration thus assisting the shear crack formation. Fiber breaks were found in only one disk which had failed after 1600 cycles at 0.0072 cyclic strain range. These fiber breaks were not in localities of maximal biaxial tensile loading. It is doubtful that the observed fiber breaks were formed during the biaxial fatigue.

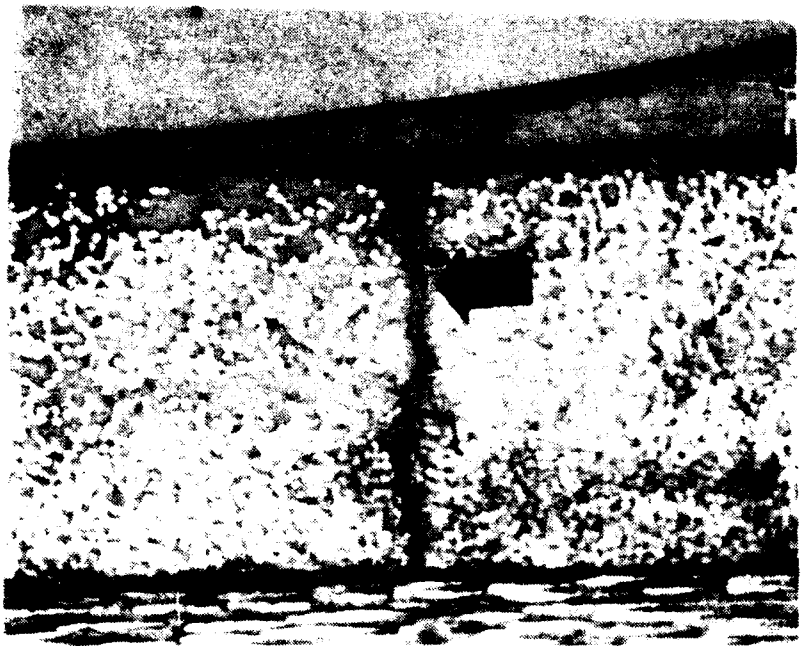

(a)

(b)

Figure 7. Maxtrix cracks.

Figure 8. Debonded area.

Ultrasonic examination of failed disks identified some delaminations. An ultrasonic scan of a disk with a delamination is shown in Figure 9. The delamination formed after 45,500 cycles at a cyclic strain range of 0.0042. The damaged area is off the disk's center and is elongated along the 90^0 fibers. In some disks which had failed in fatigue, more than one shear crack had formed. The white areas shown in the C-scan of Figure 10 represent delaminations which are not all coplanar and were generated after 1100 cycles at a cyclic biaxial tensile strain range of 0.0072. The delaminations caused the maximal cyclic load to decrease from 1.8 KN to 1.3 KN (28% decrease). The cracks shown in Figure 7 and the debonded areas of Figure 8 were not detected by our X-ray, ultrasonic scanning, or Eddy current efforts. Fiber fractures were readily detected by De Goeje and Wapanaar (4) with an Eddy current method. It is noted here that their method uses high frequencies (30 MHz) and is successful when at least 8% of the total composite's thickness bears fiber cracks. Since a limited number of fiber breaks were found in the failed disks, it is not surprising that our Eddy current efforts were not successful.

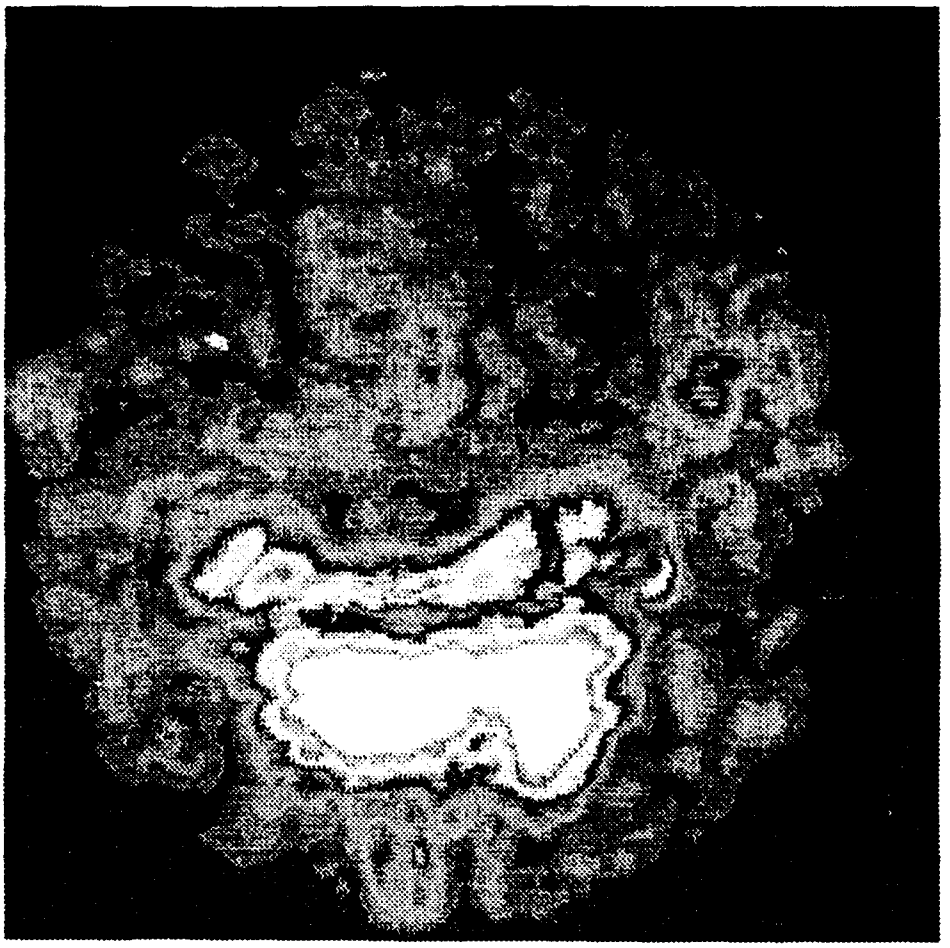

Figure 9. Ultrasonic scan with single delamination.

Discussion

The response of the resin composite to biaxial tensile loading during a single cycle is depicted in Figure 2. As with the aluminum composite (1), some hysterisis was also noticed on unloading the resin composite (not shown in Figure 2). However, unlike the metal matrix composite, no residual strain was noted with the organic composite after unloading from strain as high as 0.0067. The presence of a hysterisis loop and the absence of residual strain witness a viscoelastic composite behavior below the 0.0067 strain. However, the original curve was resumed after the load instability with continuing loading, unloading from strains greater than 0.0067 resulted in a residual strain. The latter strain was the result of composite damage. Other differences in the one cycle behavior of the two composites pertain to the shape of the loading curve and the failure mechanisms. The metal matrix composite exhibited an initial linear curve which was followed by a segment of decreasing slope. The strain at which this change was observed to begin was 0.009 which is 100% of the composite's uniaxial tensile strain to failure. Beyond this point, further increase in load would cause fiber breaks under biaxial flexural loading which, in turn, would cause the slope of the curve to decrease.

The organic composite exhibited an elastic behavior up to a strain of 0.0067 which is 43% of the composite's strain to failure under uniaxial tension. Since the carbon fibers' tensile strain to failure is 0.0165 (see Table 1), no fiber breaks were expected to form in the organic composite under biaxial flexural loading. The dominant failure mechanism for the organic composite was matrix cracking parallel to the plies and usually forming at the interface of the 0^{o} and the 90^{o} plies and in the tensile sides of the disks. The shape of the curve for the organic composite was convex downward which was indicative of a stiffening response. This stiffening is characteristic of carbon filaments (5) and organic composites reinforced with carbon fibers (6,7). Comparing the strains to failure under biaxial flexural tensile loading, the metal matrix composite presents a slightly higher failure strain.

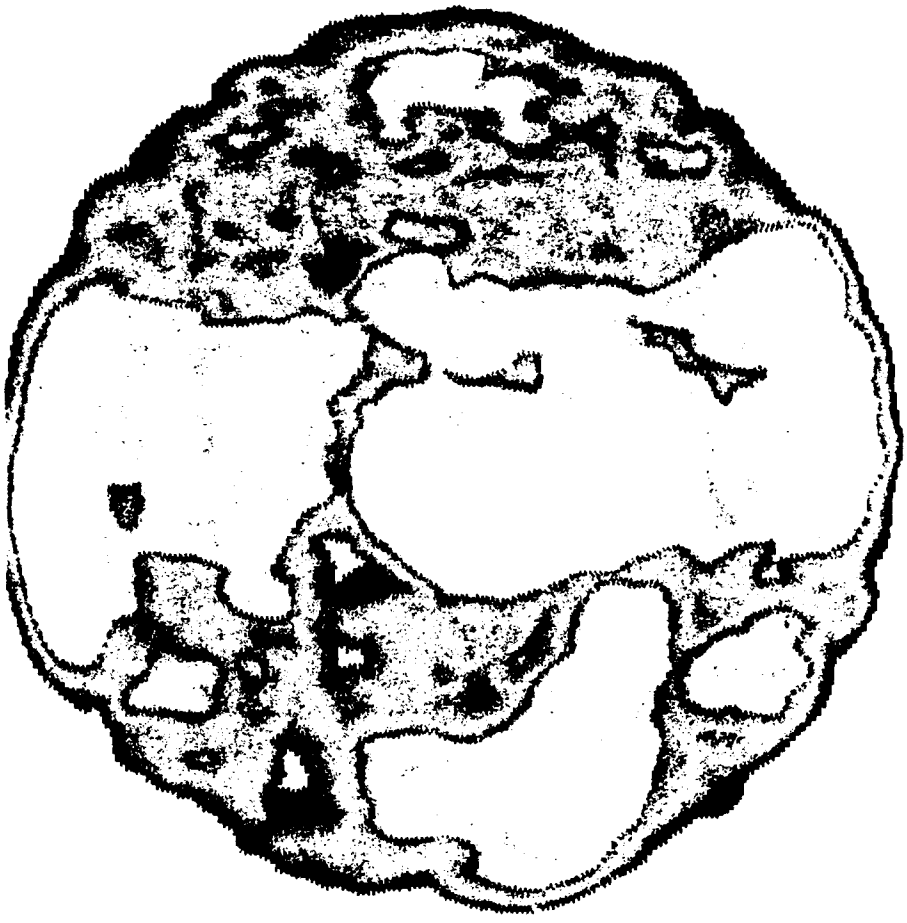

Figure 10. Ultrasonic scan with multiple delaminations.

The cyclic biaxial response of the organic composite presented a decisive superiority over that of the metal matrix composite. The organic composite exhibited a biaxial tensile strain endurance limit of 0.003 which is more than twice the magnitude of the endurance limit of the metal matrix composite (0.00132). The life span of the aluminum composite at a cyclic strain range of 0.003 is less than 10^{3} cycles (1); this is very short compared to the 10^{6} cycles for the organic composite. It is noted, however, that when

the strain endurance limits are expressed as percentages of the respective uniaxial monotonic tensile strains to failure, the result is similar for both composites. These percentages are 19% and 15% for the organic and the metal matrix composites, respectively. The properties of the two composites are listed in Table 4 for comparison.

Table 4. Composite mechanical properties

Parameter	SiC/Al-Ref (1)	Gr/ep Composite
E_{11} (GPa)	136	73.6
UTS (MPa)	629	1112
e_f (uniaxial, monotonic)	0.009	0.0155
e_f (biaxial, monotonic)	0.009	0.0067
e_N (biaxial, cyclic)	0.00132	0.003

Matrix *shear cracks* (see Figure 4) were formed under monotonic biaxial tensile loading in the resin composite at strains e_{xx} as small as 0.0067. The same type of cracks formed under cyclic biaxial tensile loading at strain ranges reaching a minimal of 0.003. In the metal matrix composite (1), *shear cracks* formed in the aluminum matrix under cyclic loading only. This could indicate that the stronger aluminum matrix resisted the formation of *shear cracks* under monotonic biaxial tensile loading. It is noted that shear cracks were not confined in the tension side of the disk during flexure. In the aluminum composite, shear cracks also formed in the compression sides of some disks.

The strain e_{xx} is sensitive to local events; e.g., matrix yielding or cracking, while the displacement **W** represents the overall reaction of the composite disk. Thus, depending upon the location, size, and nature of the generated damage, the strain and the displacement will react disproportionally. While the relationship between the displacement and the strain in the organic composite was linear (see Figure 5) up to high strains (0.0067), the contrary was true for the aluminum composite (1). The latter composite presented some residual strain after unloading due to the local inelastic response of the aluminum matrix. This aluminum inelastic response was triggered by high residual stresses which were locked in the composite after its thermal processing. The linearity of the relationship in the organic composite assumes, however, that no significant damage was introduced in the material during loading. Here, the term *significant* implies detectable by the load, strain, and displacement monitoring instrumentation. Relationships like the one shown in Figure 5 could prove to be very useful in applications such as smart composite structures. Using appropriate algorithms, the relationships could provide information about the integrity of composite structures.

The only defect which was identified nondestructively was the delamination. Several delaminations were detected by ultrasonic C-scanning. Matrix cracks were detected and imaged ultrasonically with a spherically focused transducer by Michael R. Gorman (8). Because equipment for Polar Backscatter Imaging was not available, matrix cracks were not detected by our ultransonic efforts. The X-ray radiography and the Eddy current examination did not identify the damage which was generated in the composite disks during their biaxial loading. However, transverse matrix cracks have been detected with

X-rays in graphite/epoxy laminates by Daniel and Lee (3). Daniel and Lee used a solution of zinc iodide to enhance the X-ray image. Given that the Eddy current method is sensitive to fiber breaks only, and since limited fiber breaks formed in our organic composite, it is not surprising that our efforts with this latter method were not successful.

Future work on the biaxial flexural specimen will include examination of the effects of the disk's thickness and radius on the extent and shape of the tensile strain fields.

Conclusions

The response of the carbon fiber/epoxy, cross-ply composite to biaxial flexural, and tensile loading was assessed using disk specimens. Under biaxial flexural loading, the formation of delaminations resulted in failure at a strain of 0.0067. This strain is only 43% of the composite's strain to failure under uniaxial tension. Under cyclic, biaxial, tensile loading, and for 10^6 cycles of fatigue life, the composite's useful cyclic strain range was limited to 0.003. The latter strain is only 19% of the composite's uniaxial tensile strain to failure. Fatigue failure mechanisms included delaminations and, to a lesser extent, matrix cracks and, possibly, fiber bundle debonds.

Acknowledgment

The authors wish to express their gratitude to Ms. Elizabeth Goeke for her advice and assistance on the technicalities of the project.

References

1. TSANGARAKIS, N., PEPI, M. S. *Biaxial Flexing of a Fiber Reinforced Aluminum Composite*. J. of Compo. Mat., v. 24, no. 7, July 1990, p. 770-785.
2. CAMPONESCHI, E. T., Jr. *Though-Thickness Strain Response of Thick Composites in Compression*. Sagamore U.S. Army Materials Research Conference Proceedings, 23-26 October 1989, Plymouth, MA, p. 185-210.
3. DANIEL, I. M., LEE, J. W. *Damage Development in Composite Laminates Under Monotonic Loading*. J. Compo. Techn. and Res., v. 12, no. 2, 1990, p. 98-102.
4. DeGOEJE, M. P., and WAPENAAR, K. E. D. *Non-Destructive Inspection of Carbon Fibre Reinforced Plastics Using Eddy Current Methods*. Composites, v. 23, no. 3, May 1992, p. 147-157.
5. CURTIS, G. J., MILNE, J. M., and REYNOLDS, W. N. *Non-Hookean Behavior of Strong Carbon Fibers*. Nature, v. 220, December 1968, p. 87-88.
6. PINDERA, J. J., HERAKOVICH, C. T. *An Elastic Potential for the Nonlinear Response of Unidirectional Graphite Composites*. J. of Appl. Mech., v. 51, September 1984, p. 546-550.
7. ISHIKAWA, T., MATSUSHIMA, M., and HAYASHI, Y. *Hardening Non-Linear Behavior in Logitudinal Tension of Unidirectional Carbon Composites*. J. Mat. Sci., v. 20, 1985, p. 4075-4083.
8. GORMAN, M. R. *Ultrasonic Polar Backscatter Imaging of Transverse Matrix Cracks*. J. Compo. Mat., v. 25, November 1991, p. 1499-1514.

DISTRIBUTION LIST

No. of Copies	To
1	Office of the Under Secretary of Defense for Research and Engineering, The Pentagon, Washington, DC 20301
	Director, U.S. Army Research Laboratory, 2800 Powder Mill Road, Adelphi, MD 20783-1197
1	ATTN: AMSRL-OP-CI-AD, Technical Publishing Branch
1	AMSRL-OP-CI-AD, Records Management Administrator
	Commander, Defense Technical Information Center, Cameron Station, Building 5, 5010 Duke Street, Alexandria, VA 22304-6145
2	ATTN: DTIC-FDAC
1	MIA/CINDAS, Purdue University, 2595 Yeager Road, West Lafayette, IN 47905
	Commander, Army Research Office, P.O. Box 12211, Research Triangle Park, NC 27709-2211
1	ATTN: Information Processing Office
	Commander, U.S. Army Materiel Command, 5001 Eisenhower Avenue, Alexandria, VA 22333
1	ATTN: AMCSCI
	Commander, U.S. Army Materiel Systems Analysis Activity, Aberdeen Proving Ground, MD 21005-5066
1	ATTN: AMXSY-MP, H. Cohen
	Commander, U.S. Army Missile Command, Redstone Arsenal, AL 35809
1	ATTN: AMSMI-RD-CS-R/Doc
	Commander, U.S. Army Armament, Munitions and Chemical Command, Dover, NJ 07801
2	ATTN: Technical Library
	Commander, U.S. Army Natick Research, Development and Engineering Center, Natick, MA 01760-5010
1	ATTN: Technical Library
	Commander, U.S. Army Satellite Communications Agency, Fort Monmouth, NJ 07703
1	ATTN: Technical Document Center
	Commander, U.S. Army Tank-Automotive Command, Warren, MI 48397-5000
1	ATTN: AMSTA-ZSK
1	AMSTA-TSL, Technical Library
	Commander, White Sands Missile Range, NM 88002
1	ATTN: STEWS-WS-VT
	President, Airborne, Electronics and Special Warfare Board, Fort Bragg, NC 28307
1	ATTN: Library
	Director, U.S. Army Research Laboratory, Weapons Technology, Aberdeen Proving Ground, MD 21005
1	ATTN: AMSRL-WT
	Commander, Dugway Proving Ground, UT 84022
1	ATTN: Technical Library, Technical Information Division
	Commander, U.S. Army Research Laboratory, 2800 Powder Mill Road, Adelphi, MD 20783
1	ATTN: AMSRL-SS
	Director, Benet Weapons Laboratory, LCWSL, USA AMCCOM, Watervliet, NY 12189
1	ATTN: AMSMC-LCB-TL
1	AMSMC-LCB-R
1	AMSMC-LCB-RM
1	AMSMC-LCB-RP
	Commander, U.S. Army Foreign Science and Technology Center, 220 7th Street, N.E., Charlottesville, VA 22901-5396
3	ATTN: AIFRTC, Applied Technologies Branch, Gerald Schlesinger
	Commander, U.S. Army Aeromedical Research Unit, P.O. Box 577, Fort Rucker, AL 36360
1	ATTN: Technical Library

No. of Copies	To
	U.S. Army Aviation Training Library, Fort Rucker, AL 36360
1	ATTN: Building 5906-5907
	Commander, U.S. Army Agency for Aviation Safety, Fort Rucker, AL 36362
1	ATTN: Technical Library
	Commander, Clarke Engineer School Library, 3202 Nebraska Ave., N, Fort Leonard Wood, MO 65473-5000
1	ATTN: Library
	Commander, U.S. Army Engineer Waterways Experiment Station, P.O. Box 631, Vicksburg, MS 39180
1	ATTN: Research Center Library
	Commandant, U.S. Army Quartermaster School, Fort Lee, VA 23801
1	ATTN: Quartermaster School Library
	Naval Research Laboratory, Washington, DC 20375
2	ATTN: Dr. G. R. Yoder - Code 6384
	Chief of Naval Research, Arlington, VA 22217
1	ATTN: Code 471
	Commander, U.S. Air Force Wright Research & Development Center, Wright-Patterson Air Force Base, OH 45433-6523
1	ATTN: WRDC/MLLP, M. Forney, Jr.
1	WRDC/MLBC, Mr. Stanley Schulman
	U.S. Department of Commerce, National Institute of Standards and Technology, Gaitherburg, MD 20899
1	ATTN: Stephen M. Hsu, Chief, Ceramics Division, Institute for Materials Science and Engineering
1	Committee on Marine Structures, Marine Board, National Research Council, 2101 Constitution Avenue, N.W., Washington, DC 20418
1	Materials Sciences Corporation, Suite 250, 500 Office Center Drive, Fort Washington, PA 19034
1	Charles Stark Draper Laboratory, 555 Technology Square, Cambridge, MA 02139
	Wyman-Gordon Company, Worcester, MA 01601
1	ATTN: Technical Library
	General Dynamics, Convair Aerospace Division P.O. Box 748, Forth Worth, TX 76101
1	ATTN: Mfg. Engineering Technical Library
	Plastics Technical Evaluation Center, PLASTEC, ARDEC Bldg. 355N, Picatinny Arsenal, NJ 07806-5000
1	ATTN: Harry Pebly
1	Department of the Army, Aerostructures Directorate, MS-266, U.S. Army Aviation R&T Activity - AVSCOM, Langley Research Center, Hampton, VA 23665-5225
1	NASA - Langley Research Center, Hampton, VA 23665-5225
	U.S. Army Vehicle Propulsion Directorate, NASA Lewis Research Center, 2100 Brookpark Road, Cleveland, OH 44135-3191
1	ATTN: AMSRL-VP
1	NASA - Lewis Research Center, 2100 Brookpark Road, Cleveland, OH 44135-3191
	Director, Defense Intelligence Agency, Washington, DC 20340-6053
1	ATTN: ODT-5A (Mr. Frank Jaeger)
	Commander, U.S. Army Research Laboratory, Watertown, MA 02172-0001
2	ATTN: AMSRL-OP-CI-D, Technical Library
10	Authors